Theory of surface vibrations in epitaxial thin films

N. S. Luo,* P. Ruggerone,† and J. P. Toennies
Max-Planck-Institut für Strömungsforschung, Bunsenstrasse 10, 37073 Göttingen, Germany
(Received 27 June 1995; revised manuscript received 16 January 1996)

Recent inelastic helium atom scattering measurements of the phonon dispersion curves of epitaxial thin films (2–30 ML) of four different types of systems are analyzed within the framework of a force constant model. Whereas Na/Cu(001) shows nearly flat dispersionless modes with frequencies at the Γ point that follow the open standing wave sequence, the other systems Pb/Cu(111), Ar(Kr)/Ag(111), and KBr/NaCl(001) reveal a more complex behavior. These qualitative differences can be explained in terms of a simple linear chain model in which the behavior is determined by the strength of the force constant coupling of the thin films to the substrate relative to the force constant within the films. Detailed slab calculations for Na/Cu(001) confirm this model and indicate that the observed flat phonon dispersion curves are related to the strength of the interface interaction and bcc structure of the epitaxially grown Na thin films. [S0163-1829(96)05728-1]

I. INTRODUCTION

With the development of molecular beam epitaxial (MBE) growth techniques in research and technology, the physical and chemical properties of epitaxial thin films are currently being studied in great detail by various experimental and theoretical methods.[1,2] This research is motivated by a desire to understand the large variety of physical properties in epitaxial film systems, which are associated not only with essential characteristics of the epitaxial material, such as quantum size effects, but also with interface interactions between the epitaxial film and the underlying substrate. Many experiments have so far been carried out to detect the structural, vibrational, and electronic properties of thin film systems. The effect of quantum-size restrictions on electronic states have been observed in photoemission,[3–10] optical second harmonic generation,[8,9] high-resolution electron energy-loss spectroscopy,[9,11] electron tunneling,[12,13] reflection high-energy electron diffraction,[14] and helium atom scattering[15] (HAS) experiments. Because of the stress induced not only by the structural mismatch[16–19] but also by electronic interface interactions,[6,7,20] an epitaxially grown system is expected to show large deviations in the vibrational properties compared to the bulk. The first successful inelastic He scattering measurements of epitaxially deposited films were reported by Gibson and Sibener[21,22] in 1985. For MBE grown overlayers (1, 2, 3, and 25 ML) of heavy rare gases on a Ag(111) surface they were able to measure the layer-by-layer evolution of the surface-phonon dispersion relations for rare-gas films physisorbed on Ag(111) across the entire surface Brillouin zone (SBZ). At the Γ point, the frequency of the mode that evolves into the Rayleigh wave decreases monotonically as the film thickness increases, falling as expected to zero in the limit of infinite thickness. For the rare-gas atoms, the Ag(111) surface appears to be nearly perfectly smooth with a potential barrier between adjacent sites of only about 30 meV.[23] Thus it is a good approximation to assume that the substrate provides only a physisorption holding potential directed normal to the surface $V(z)$, which binds the rare-gas atoms to the underlying substrate surface plane. Similar results have since been reported for Ar, Kr, and Xe on Pt(111),[24,25] and have also been analyzed using force constant models.[25]

Measurements of thin-film phonons also have been carried out using EELS for the following metal systems: Ag/Ni(001),[26] Fe/Cu(001),[27] Co/Cu(001),[28] and Ni/Cu(001).[29–31] In all cases only a few modes could be observed and no loss peaks were found at the zone center. The magnetic films Fe/Cu(001) and Ni/Cu(001) differ from the other systems and those to be discussed here in that the layers are stiffer than the substrate.[32] Recently, for a number of epitaxially grown films HAS phonon measurements have provided complete dispersion curves including the Γ point. For example, in one recent study by Safron *et al.*[33] of films of 2, 3, 4, and 7 ML of KBr on NaCl(001) well-defined peaks were observed, which were attributed to Rayleigh-like modes. At the Γ point the Rayleigh mode exhibited a distinct gap, which decreased with increasing overlayer thickness. However, in more recent HAS investigations of surface phonons in epitaxially grown Na films on a Cu(001) substrate an entirely different behavior was reported by Benedek *et al.*[34] For these very soft Na films nearly dispersionless phonon modes were observed starting at the Γ point for thicknesses varying from 2 to 30 ML. The modes were attributed to standing waves with longitudinal polarization directed perpendicular to the film surface. Between 2 and 20 ML the frequencies of the standing waves at the Γ point are very well approximated by the following expression:

$$\omega_n(N) = \frac{2n-1}{N}\frac{\pi v}{2a^*}, \quad n=1,2,\ldots,N, \tag{1}$$

corresponding to an open-ended standing wave harmonic sequence, which was referred to as ''organ-pipe'' modes. Here, N is the number of monolayers, v a phase velocity, and a^* an effective interplanar spacing. Surprisingly a similar HAS study of Pb/Cu(111) (Ref. 35) did not show the open standing wave sequence but rather a dispersive behavior similar to that found for Ar(Kr)/Ag(111) and the insulator system discussed above.

The experimental lowest frequencies $\omega_1(N)$ at the Γ point for these four different types of epitaxial multilayer systems

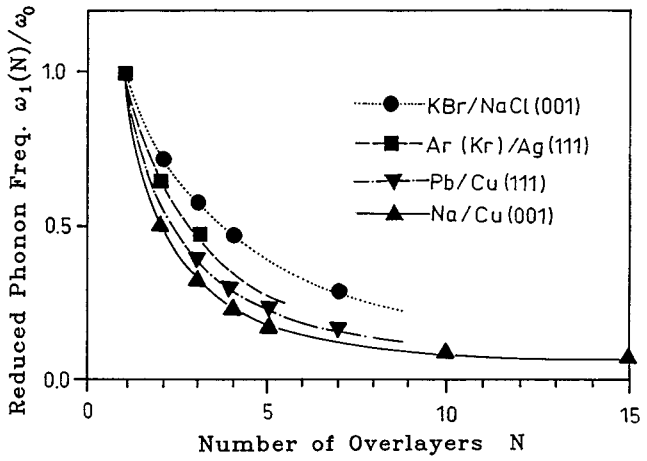

FIG. 1. The lowest measured frequencies $\omega_1(N)$ at the $\bar{\Gamma}$ point normalized by the measured or assumed vibrational frequency ω_0 ($\omega_0=\sqrt{K_f/m_o}$) of a single monolayer are plotted vs the number of the overlayers N for Na/Cu(001), KBr/NaCl(001), Pb/Cu(111), and Ar(Kr)/Ag(111) systems.

versus the number of overlayers N are shown in Fig. 1. Some important physical properties of these systems are collected for later reference in Table I. As seen in Fig. 1 the lowest shear vertical vibrational frequency $\omega_1(N)$ of the Na/Cu(001) system at the Γ point varies with the number of Na monolayers as N^{-1} as expected from Eq. (1). However, for Ar(Kr)/Ag(111), KBr/NaCl(001), and Pb/Cu(111) the open standing wave law Eq. (1) does not apply. For example, a similar plot of the experimental data of 2-, 3-, 4-, and 7-ML KBr overlayers on NaCl(001) shows a decrease of the lowest frequencies $\omega_1(N)$ proportional to $N^{-1/2}$. In the case of the Ar(Kr)/Ag(111) multilayer systems (1–3 ML) the lowest frequencies $\omega_1(N)$ at the Γ point are found to be proportional to $N^{-\gamma}$, with $\gamma=0.85$, which is very similar to the value of $\gamma=0.89$ for the Pb/Cu(111) multilayer system. Thus, in these four different epitaxial systems the Γ-point frequencies for each system have a characteristic functional dependence on the film thickness $N^{-\gamma}$ with γ between 0.5 and 1.0. In addition, alkalis on graphite,[44] NaCl/Ge(001),[45] Pb/Ge(111),[46] and NiO/Ag(001) (Ref. 47) have recently been investigated with helium atom scattering. We have not analyzed these data here since for the alkalis on graphite no shear vertical modes at the Γ point were found, while for NaCl/Ge(001) and NiO/Ag(001) the measured data at the Γ point are still too sparse to determine an accurate dependence on overlayer number N, and for the Pb/Ge(111) system a behavior similar to Pb/Cu(111) was observed. It is indeed surprising that so far only the Na/Cu(001) system exhibits the open standing wave (organ-pipe) sequence in the vibrational frequencies.[48]

In view of these differences and the novelty of these systems we have adopted a simple Born–von Karman force constant model in an initial attempt at understanding these effects. Of course, we realize that recent HAS studies of phonons on the transition-metal surfaces have shown that it is also important to explicitly include the electronic degrees of freedom in describing phonons in metals.[49–51] However, these effects are not expected to be of great importance for insulator systems nor for nearly free electron metals[52] with the possible exception of Pb/Cu(111), which is presently under detailed study.[53]

This paper is organized as follows. In Sec. II we first present a systematic theoretical analysis of the surface vibrational properties at the Γ point for all the above-mentioned epitaxial film systems, within the framework of a one-dimensional force constant model. In order to gain insight into the dispersion curves of the vibrations polarized normal to the surface as the wave vector approaches the zone boundary, this model is extended to a three-dimensional slab. In Sec. III we present a three-dimensional slab calculation for the Na/Cu(001) system and compare the results to the available experimental data. We test the rigid substrate assumption and discuss the influence of acoustic impedance mismatches to the surface phonon densities of states of the thin films for this system. Finally, a brief conclusion summarizes the main points of this investigation. A preliminary account was reported in Ref. 54.

TABLE I. Some important physical properties of materials for the four epitaxial systems considered. ρ (g/cm^3) is the mass density, B (10^{11} dyn/cm^2) the bulk modulus, ω_M (meV) the maximum bulk phonon frequency. α is the direction normal to the surface of the epitaxial system, v_α (10^5 cm/s) and Z (10^5 g/cm^2 s) are the longitudinal sound velocity and acoustic impedance ($Z=\rho v_\alpha$) in this direction, respectively.

Materials	Structure	ρ[a]	B	ω_M	α	v_α[a]	Z
Ar	fcc	1.65	0.27[b]	8.49[c]	[111]	1.44	2.38
Kr	fcc	3.4	0.35[d]	6.21[c]	[111]	1.47	4.99
Ag	fcc	10.49	9.93[a]	22.0[e]	[111]	3.97	41.65
KBr	fcc	2.75	1.6[a]	20.9[c]	[001]	3.55	9.76
NaCl	fcc	2.16	2.5[a]	32.1[c]	[001]	4.75	10.26
Na	bcc	0.97	0.52[a]	15.66[f]	[110]	3.91	3.79
Cu	fcc	8.95	13.9[a]	29.78[g]	[001]	4.33	38.75
Pb	fcc	11.48	4.34[a]	9.03[h]	[111]	2.32	26.63
Cu	fcc	8.95	13.9[g]	29.78[g]	[111]	5.15	46.09

[a]Reference 36.
[b]Reference 37.
[c]Reference 39.
[d]Reference 38.
[e]Reference 40.
[f]Reference 41.
[g]Reference 42.
[h]Reference 43.

II. SYSTEMATIC THEORETICAL ANALYSES

A. The linear chain on a rigid substrate

At the Γ point, the vibrations of a multilayer system are simplest to describe since all the atoms within a given layer vibrate with the same phase and amplitude, and there is no mixing between vibrations polarized normal and parallel to the surface. Therefore, at the Γ point the multilayer system can be considered in the same way as the usual textbook problem of a linear chain of atoms, where the force constants describe the coupling between the layers.[55] The equation of motion of this one-dimensional system can be written as

$$m_l \frac{d^2 u_{\alpha l}}{dt^2} = -\sum_{l'} K_{\alpha,ll'} u_{\alpha l'}, \tag{2}$$

where $u_{\alpha l}$ is the displacement function of the atom in the lth plane along the α Cartesian direction, m_l is the mass of an atom in the lth plane, and $K_{\alpha,ll'}$ is the effective force constant between the lth and l'th planes for vibrations in the α direction, which in the present case is directed normal to the surface of the epitaxial film. The effective interplanar force constant can be expressed as

$$K_{\alpha,ll'} = -\sum_{n'} \Phi_{\alpha\alpha}(0l;n'l'), \tag{3}$$

where $\Phi_{\alpha\alpha}(0l;n'l')$ is the interatomic force constant matrix element describing the interactions between the $0l$th and $n'l'$th atoms vibrating along the α direction. Here $n'l'$ denotes the n'th atom in the l'th plane, 0 the reference atom in the lth plane, and the sum is over all the n' atoms in the l'th plane. For two-body central potentials, the interatomic force constant matrix elements can be expressed in terms of the radial force constants $\beta(R)$ and the tangential force constants $\alpha(R)$.[56,57] Thus, the effective interplanar force constants for $l \neq l'$ are given by

$$K_{\alpha,ll'} = \sum_{n'} \left[\frac{R_\alpha^2}{R^2} \beta(R) + \left(1 - \frac{R_\alpha^2}{R^2}\right) \alpha(R) \right] \tag{4a}$$

and from translational invariance

$$K_{\alpha,ll} = -\sum_{l' \neq l} K_{\alpha,ll'}, \tag{4b}$$

where R is the distance between the $0l$th and $n'l'$th atoms, and R_α is the corresponding component of $\mathbf{R}$ in the α direction. The functional dependence of β and α on R takes account of whether nearest-neighbor or next-nearest-neighbor, etc., interactions are included.

To achieve a general and systematic analysis, we consider a linear chain of N atomic layers with an effective nearest-neighbor interplanar force constant K_0. For simplicity, we start by considering the substrate as a rigid wall (model A), and label the interplanar interface force constant with K_f [see Fig. 2(a)]. The solution of the equation of motion with a free boundary at $l=N$ and a fixed boundary at $l=0$ consists of the superposition of two waves with amplitudes $u_>$ and $u_<$ traveling in opposite directions with the phase angles $+q_z l$ and $-q_z l$ ($q_z = ka^*$, where k is the wave vector, a^* the spacing between the adjacent planes), respectively,

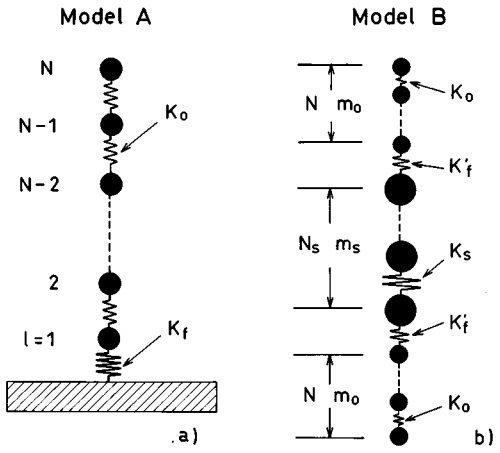

FIG. 2. The schematic diagram (a) of model A of a linear chain on a rigid substrate and (b) of model B of a linear chain with a soft substrate. Both models are for the vertical vibrations at the Γ point in the epitaxial films.

$$u_l = (u_> e^{iq_z l} + u_< e^{-iq_z l}) e^{i\omega t}, \tag{5}$$

where $l=1,2,\ldots,N$. In contrast to an infinite chain in which the phase angle is continuous, here the phase angle is discrete. In Eq. (5) q_z is assumed to be the lowest root, which has to be determined from the boundary conditions. If the displacement function of Eq. (5) is substituted into Eq. (2) for $l=2,3,\ldots,N-1$ (i.e., neglecting the displacements of the particles at the boundaries), we obtain the same solution as for a linear chain,

$$4K_0 \sin^2(q_z/2) = m\omega^2, \tag{6}$$

where m is the mass of an atom in the chain, and q_z is discrete.

In order to obtain a solution that also describes the motion of the atoms at both ends of the chain at $l=N$ and $l=1$, we find that it is expedient to assume that the atom at $l=N$ has the same amplitude as a fictitious atom at $l=N+1$.[54] This leads to the condition

$$\begin{aligned} u_N &= [u_> e^{iq_z N} + u_< e^{-iq_z N}] e^{i\omega t} \\ &= [u_> e^{iq_z N} e^{iq_z} + u_< e^{-iq_z N} e^{-iq_z}] e^{i\omega t} = u_{N+1}, \end{aligned} \tag{7}$$

with the solution $u_< = u_> e^{iq_z(2N+1)}$. Substituting it into Eq. (5) the displacement function is now given by

$$u_l = u_> e^{i\omega t} [e^{iq_z l} + e^{-iq_z}(l-2N-1)]. \tag{8}$$

Substituting Eq. (8) into Eq. (2) for both $l=1$ and $l=N$ we then get

$$2\sin(q_z/2)\sin(q_z N) = (K_f/K_0)\cos[q_z(N-\tfrac{1}{2})]. \tag{9}$$

For $q_z \to 0$, Eq. (9) reduces to

$$N q_z^2 = K_f/K_0. \tag{10}$$

Then we can use Eq. (6) to obtain the following expression for the frequencies corresponding to wavelengths satisfying Eq. (10) as a function of N:

$$\omega_1^2(N) = K_0 q_z^2/m = K_f/(Nm). \tag{11}$$

This equation implies that all the atoms in the chain move in unison with a total effective mass Nm.

To solve Eq. (9) in general it is useful to rewrite it as

$$(2-K_f/K_0)\sin(q_z/2)\sin(q_zN) = (K_f/K_0)\cos(q_z/2)\cos(q_zN). \quad (12)$$

For the special case of $K_f/K_0=2$, this equation has the simple solution $\cos(q_zN)=0$, which requires

$$q_z=\frac{2n-1}{2N}\,\pi, \quad (13)$$

where $n=1,2,3,\ldots,N$. As before we substitute Eq. (13) into Eq. (6) to obtain

$$\omega_n(N)=\omega_M\,\sin\left[\frac{2n-1}{2N}\,\frac{\pi}{2}\right], \quad (14)$$

where $\omega_M=\sqrt{2K_f/m}$. For the lower-order ($n\ll N$) vibrations, Eq. (14) can be written approximately as

$$\omega_n(N)\approx\omega_M\left[\frac{2n-1}{2N}\,\frac{\pi}{2}\right]. \quad (15)$$

This is just the case of open standing wave modes.[34] In addition, for the lower-order roots (small n) the phonon dispersion curve is approximately linear. The phase velocity can be derived from Eq. (6) as

$$v=\frac{d\omega}{dk}=\sqrt{\frac{4K_0}{m}}\frac{a^*}{2}\cos\left(\frac{q_z}{2}\right)=\omega_M\,\frac{a^*}{2}\cos\left(\frac{q_z}{2}\right)\approx\omega_M\,\frac{a^*}{2}. \quad (16)$$

Therefore, Eq. (15) is consistent with Eq. (1) obtained by continuum theory. Thus within the framework of the force constant model, $K_f/K_0=2$ is the force constant condition for the appearance of the open standing wave modes in a multilayer system.

From this model of a one-dimensional chain on a rigid substrate, we can now understand the differences between the experimental data at the Γ point for KBr/NaCl(001), Na/Cu(001), Pb/Cu(111), and Ar(Kr)/Ag(111) multilayer systems. According to Eq. (9) the relation between the vibrational frequencies and the overlayer thickness depends sensitively on the ratio (K_f/K_0) between the interface and interplanar force constants. In one limit the coupling to the substrate is negligible, i.e., K_f is very small ($K_f/K_0\ll 2$); in the lowest-frequency vibrational modes all the atoms of the overlayers move in unison and the corresponding frequencies $\omega_1(N)$ are just proportional to $1/\sqrt{N}$. This represents the case of the KBr/NaCl(001) system. The other extreme occurs when the coupling to the substrate is strong and K_f/K_0 is equal to about 2. In this limit the amplitudes are almost zero at the interface, and vary throughout the film according to the open standing wave behavior, as in the case of Na on Cu(001). The cases of Ar(Kr)/Ag(111) and Pb/Cu(111) are intermediate with $K_f/K_0<2$, but not too small.

To understand this general relationship in more detail, we solve Eq. (2) numerically for the simple one-dimensional interplanar force constant model with a rigid substrate. The calculated lowest frequencies $\omega_1(N)$ versus the number of epitaxial overlayers for different ratios between interface force constant K_f and film interplanar force constant K_0 are shown in Fig. 3. It is interesting to observe the striking similarity to the experimental data of Fig. 1. In all cases the frequencies decrease with increasing N due to the increase in the effective mass of the film. With increasing ratio K_f/K_0, the lowest vibrational frequencies decrease more rapidly with the number of overlayers. For very thin films ($N=1,2$), the interface coupling K_f has the greatest influence on the vibrational frequencies, especially for large K_f/K_0. For thicker films, the relative decrease in frequencies with increasing N is greatest for the largest values of K_f/K_0. If the results of Fig. 3 are plotted on a double logarithmic scale the points for $N\geqslant 2$ all fall on a straight line. Figure 4 shows the slope γ of these curves as a functions of the logarithm K_f/K_0.[58] Figure 4 suggests that a behavior similar to the open standing wave may also be found for $K_f/K_0>2$ but with $\gamma\simeq 1.1$. The more extreme situation $K_f/K_0>2$ is not considered further in this article. Table II summarizes the experimental values of γ and K_f/K_0 for the four systems in Fig. 1.

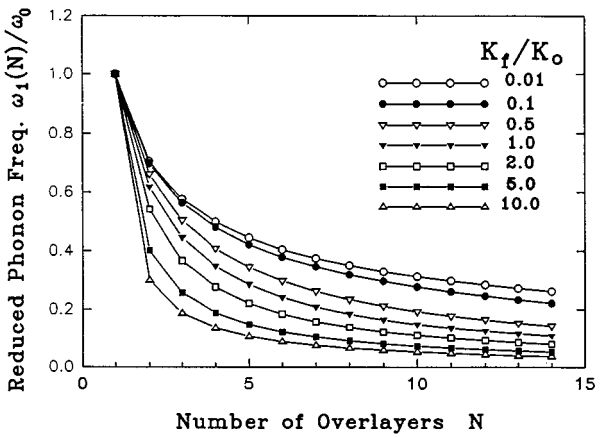

FIG. 3. The lowest calculated frequencies $\omega_1(N)$ at the $\overline{\Gamma}$ point normalized by the vibrational frequency ω_0 ($\omega_0=\sqrt{K_f/m_o}$) of a single monolayer are plotted vs the number of the overlayers N for different ratios between interface force constant K_f and intrafilm force constant K_0.

Figure 5 displays the vibrational densities of states of the atoms at the surface calculated for two different ratios of force constants $K_f/K_0=0.1$ and (corresponding to the open standing wave interface condition). The vibrational density of states at the surface is defined by the following equation:

$$\rho(\omega,N)=\sum_{j=1}^{N}|u_j(l=N)|^2\,\delta(\omega_j-\omega). \quad (17)$$

Here, ω is the frequency, ω_j is the frequency of the jth mode, and $u_j(l=N)$ is the related displacement for the surface atom $l=N$. In Fig. 5 the length of the horizontal bars at the corresponding frequency is proportional to the calculated square of the vibrational amplitude of the shear vertical motion at the surface (normal to the surface plane). One can see that the distribution of vibrational frequencies depends sensitively on the ratio K_f/K_0 between the interface and the film interplanar force constants, especially for the lowest-frequency vibrations. Generally, the lower-frequency vibrations have larger displacement amplitudes at the surface. For

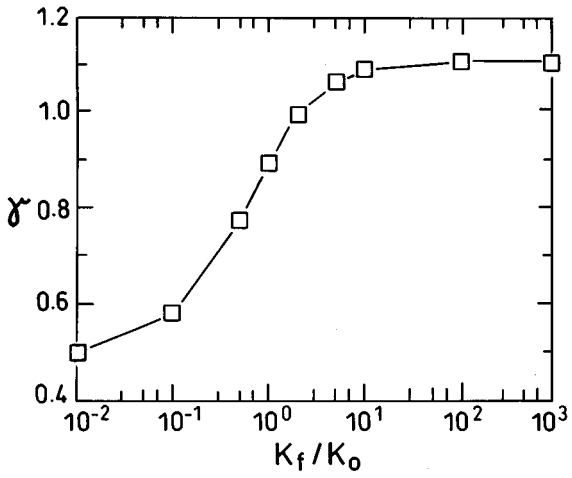

FIG. 4. The parameter γ as obtained from the slope of the logarithm of the calculated frequency of the lowest mode for $N \geq 2$ vs the logarithm of N is plotted as a function of the ratio K_f/K_0 between the interface force constant K_f and the film interplanar force constant K_0 (Ref. 58).

the open standing wave modes the amplitudes of the displacements of the surface atoms are largest in the lowest-frequency modes, especially for the thin films (N small). Since HAS is especially sensitive to the shear vertical displacements, these low-energy modes show up as strong peaks in the experimental time-of-flight spectra.

B. The linear chain on a soft substrate

In order to test the rigid substrate approximation and examine the effect of a soft substrate a more realistic model [model B, see Fig. 2(b)] is studied next. The model consists of a linear chain of N_s substrate atoms of mass m_s with N overlayer atoms of mass m_0 at each end. The nearest-neighbor interplanar force constants in the overlayer and the substrate are K_0 and K_s, respectively. The interface interplanar force constant is now labeled by K_f'. A value of 200 for N_s is chosen in order to simulate a thick substrate. A series

TABLE II. The measured functional dependence parameter γ and the fitted force constant ratio K_f/K_0 using a rigid substrate model (model A).

	KBr/NaCl(001)	Ar(Kr)/Ag(111)	Pb/Cu(111)	Na/Cu(001)
γ	0.5	0.85	0.89	1.0
K_f/K_0	0.1	0.77	1.14	2.0

of test calculations based on model B were carried out to study the error introduced by the rigid substrate approximation (model A). The vibrational dynamics of the linear chain in model B is determined by five parameters: K_0, m_o, K_f', K_s, and m_s so that the total number of possible calculations is very large. For simplicity we present only the results for the surface phonon densities of states assuming $K_s = K_0$ for two different ratios of masses $m_s/m_o = 5$ and $m_s/m_o = 1$. As in Fig. 5 the interface force constants are chosen as $K_f'/K_s = 0.1$ and $K_f'/K_s = 2$. The calculated results are shown in Figs. 6 and 7, respectively, and compared with the corresponding calculations of Fig. 5 for the rigid substrate (model A). The interplanar force constants, the atomic masses, and the corresponding acoustic impedance mismatches used in the calculations for model B are collected in Table III. The acoustic impedance mismatch is defined by $\delta = |Z_o - Z_s|/Z_s$, where Z_o and Z_s are the acoustic impedances of the overlayer and substrate materials, respectively. The acoustic impedance Z of a linear chain is proportional to $\sqrt{Km}$,[59] where K is the force constant, and m the mass of the chain atom. Thus, Figs. 5, 6, and 7 encompass both acoustic impedance mismatches of $\delta = 1.00$, 0.55, and 0 as well as different ratios of film to interface force constants.

The calculations in Figs. 6 and 7 reveal the striking differences between model A and model B. In every case the soft substrate leads to a broadening of the distribution of the phonon density of states, and the maximum amplitudes of surface phonon densities of states of the overlayer obtained for the rigid substrate are reduced accordingly. The effective error in the frequencies introduced by the rigid substrate approximation depends sensitively on the acoustic impedance

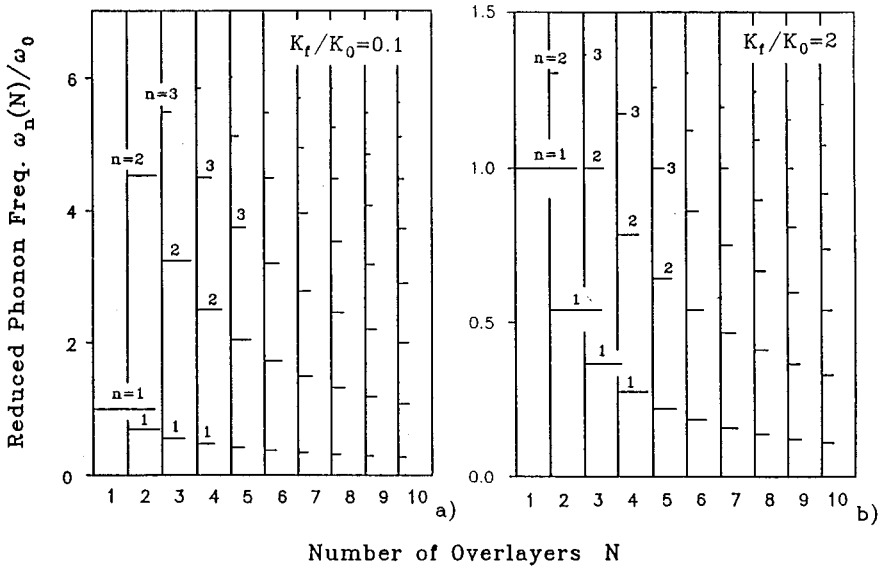

FIG. 5. Calculated vibrational densities of states at surface for the one-dimensional chains on the rigid substrate for (a) $K_f/K_0 = 0.1$ and (b) $K_f/K_0 = 2$. The frequencies are normalized by ω_0 ($\omega_0 = \sqrt{K_f/m_o}$). The horizontal bars are directly proportional to the density of states plotted from left to right.

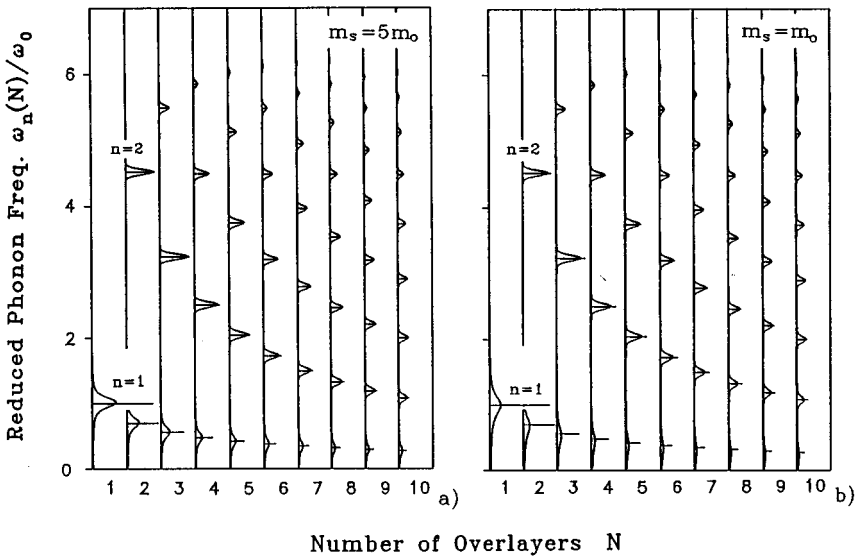

FIG. 6. Calculated vibrational densities of states at the surface for the one-dimensional chain model of a thin overlayer on a soft substrate (solid curve) in comparison with those on a rigid substrate (horizontal bars). In both (a) and (b) $K_0=K_s$, $K_f'=0.1K_0$. In (a) $m_s=5m_o$, and the impedance mismatch is $\delta=0.55$. In (b) $m_s=m_o$ and $\delta=0.0$. The frequencies are normalized by ω_0 ($\omega_0=\sqrt{K_f'/m_o}$). The horizontal bars are from Fig. 5.

mismatch and the interface force constant. When the interface force constant is very small (see Fig. 6), the substrate has only a slight influence on the peak frequency positions of the surface phonon density of states, but the peak intensities are reduced significantly, especially for the lowest-frequency modes. Thus, the ω_1 modes are especially broad. This is due to their small wave vector q_z, which means that the waves penetrate farther into the substrate and couple strongest with the substrate. Figure 7 shows calculations for an interface force constant that is twice the force constant of the film and of the substrate. In this case the lack of rigidity of the substrate has a great effect on both the frequency and the intensity distributions of overlayer surface vibrations. For the case of an intermediate mismatch (see Fig. 7) the frequencies in the soft substrate calculations are significantly shifted upwards. As in Fig. 6 the broadening of the density-of-states distribution is largest for the lowest ($n=1$) frequencies. When there is no impedance mismatch as in Fig. 7, the frequencies are shifted downwards by a large amount and the density of states vanishes almost completely. Because of the complete disappearance of mismatch the overlayer modes are almost entirely adsorbed by the substrate. They would disappear entirely if $K_f'/K_0=1$ and $m_o/m_s=1$ since in this case there is no longer an interface. As to be expected, the differences between the results for model A and model B increase with decreasing acoustical mismatch and increasing interface interaction strength. An example of a thin-film system corresponding to a small acoustic mismatch is that of the heavy alkali atoms (Cs, Rb, and K) on graphite, yet the HAS experiments did not pick up any mode at the Γ point.[44] This could well be due to smearing of the phonon density of states as illustrated in Fig. 7.

Thus the validity of the rigid substrate approximation will depend on the ratios between the acoustic impedances of the substrate and of the thin film and to some extent on the nature of the interface.[60] Table I lists the relevant physical properties (density of mass ρ, bulk modulus B, maximum phonon frequency ω_M, orientations of overlayer and substrate, longitudinal sound velocity v_α, and acoustic impedance $Z=\rho v_\alpha$) of the overlayer and substrate materials

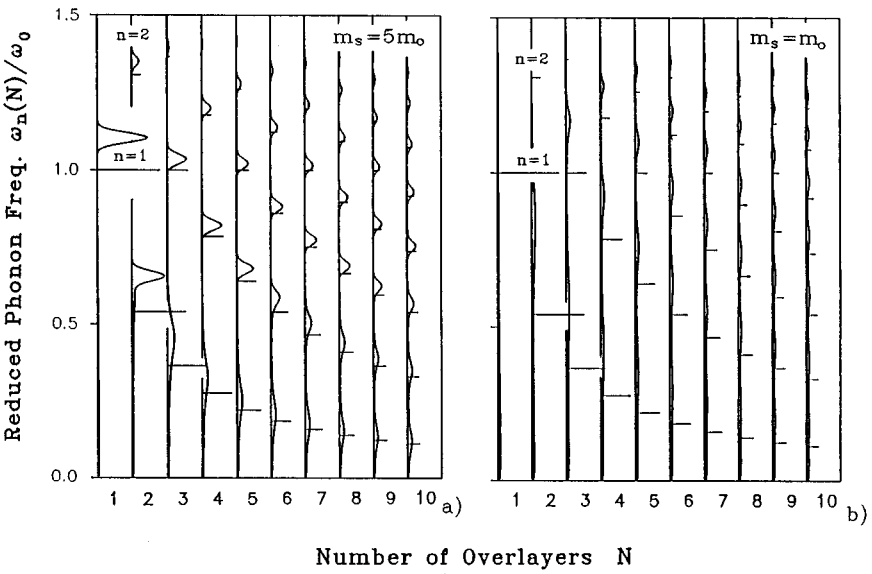

FIG. 7. Calculated vibrational densities of states at the surface for the one-dimensional chain model of a thin overlayer on the soft substrate (solid curve) in comparison with those on the rigid substrate (horizontal bars). In both (a) and (b) $K_0=K_s$ and $K_f'=2K_0$. In (a) $m_s=5m_o$, and the impedance mismatch is $\delta=0.55$. In (b) $m_s=m_o$, and $\delta=0$. The frequencies are normalized by ω_0 ($\omega_0=\sqrt{K_f'/m_o}$). The horizontal bars are from Fig. 5.

TABLE III. The chosen parameters of model B for the calculations in Figs. 6 and 7.

	K_0	m_o	K_f'	K_s	m_s	δ	
Model A	K_0	m_o	$0.1K_0$		∞	1	Fig. 5(a)
Model B	K_0	m_o	$0.1K_0$	K_0	$5m_o$	0.55	Fig. 6(a)
Model B	K_0	m_o	$0.1K_0$	K_0	m_o	0	Fig. 6(b)
Model A	K_0	m_o	$2K_0$		∞	1	Fig. 5(b)
Model B	K_0	m_o	$2K_0$	K_0	$5m_o$	0.55	Fig. 7(a)
Model B	K_0	m_o	$2K_0$	K_0	m_o	0	Fig. 7(b)

needed to apply these models to the four epitaxial systems in the present paper. Table IV lists the acoustic impedance mismatch δ and the reflection coefficient $[R=(Z_o-Z_s)/(Z_o+Z_s)]$ for the four multilayer systems. One can see that the Ar(Kr)/Ag (111) and Na/Cu(001) systems have much larger reflection coefficients at the interface than KBr/NaCl(001) and Pb/Cu(111). Therefore, the rigid substrate approximation should be a reliable assumption for the former two systems. In summary, there are in fact two conditions for the appearance of the open standing wave modes: one is a large acoustic impedance mismatch, the other is that the ratio K_f/K_0 between interface interplanar force constant K_f and intrafilm interplanar force constant K_0 is close to 2 or larger than 2.

Since both model A and model B provide qualitatively similar pictures for the frequencies of overlayer systems, K_f in model A may be looked upon as an effective coupling parameter K_f'. Thus, if the same measured frequencies versus the number of overlayers are fitted by both models, quantitative differences in the effective interface force constants appear ($K_f' \neq K_f$). The error ($\Delta=|K_f-K_f'|/K_f'$) introduced by the rigid substrate approximation depends on the acoustic impedance mismatch and the interface interaction. Only when either the acoustic impedance mismatch approaches 1 (for example, $m_s=\infty$) or the interface coupling approaches zero ($K_f=0$ and $K_f'=0$), then the substrate no longer has an effect on the overlayer vibrations, and the two models are completely equivalent.

C. Full dispersion curves for a thin film on a rigid substrate

To gain more insight into the complete dispersion curves of the shear vertical modes in thin films especially near the zone boundary, we have extended the one-dimensional force constant model to three dimensions for the example of a fcc (001) thin-film slab on a rigid substrate. For simplicity, we consider only a single nearest-neighbor atom-atom force constant β_1. According to Eq. (4), in this case the interplanar force constant for adjacent (001) planes K_0 is equal to $2\beta_1$, and the interplanar force constants to the more distant planes vanish. The results along the $\overline{\Gamma M}$ direction for two different ratios of force constants $K_f/K_0=0.1$ and 2 (corresponding to the open standing wave condition) are shown in Fig. 8(a)–8(f) for 2, 3, and 4 ML on a rigid substrate. The wave-vector range in which the vertical vibrational amplitudes on the surface are above 25% of the maximum have been emphasized in the dispersion curves by solid lines, since they are expected to show up as especially intense features in inelastic helium atom and electron impact scattering. In general phonons at wave vectors removed from the zone origin and zone boundary are no longer either only vertically or longitudinally polarized, but are a mixture of both. The complicated shape of the solid portions of the curves in Fig. 8 reflects this as well as a significant hybridization occurring when modes with different well-defined polarizations at the zone edges come near to each other at intermediate wave vectors. With increasing values of the wave vector the shear vertical polarized modes at the Γ point (indicated by V_i, $i=1,\ldots,N$) transfer their polarization by hybridization and other mixing effects to modes that at the zone origin were not polarized in the shear vertical direction.

The overall shape of the Rayleigh wave dispersion curves in Fig. 8 depends both on the interactions within the overlayer and on the interface interaction of the overlayer with the substrate. Near the Γ point, the wave vector is very small, the wavelength very long, and the substrate has a large effect on the lowest-frequency vibrations (Rayleigh wave). When the wave vector approaches the zone boundary, the vibrations become localized within the film and the effect of the substrate diminishes. Accordingly the frequencies for $K_f/K_0=0.1$ and 2.0 in Fig. 8 are very similar at the M point, whereas there are large differences at the Γ point. With increasing layer thickness, the surface is further removed from the interface and the interface coupling at the substrate influences a progressively smaller fraction of the Brillouin zone near the Γ point. It is interesting to note in both cases shown in Fig. 8 that at small wave vectors the lowest-frequency shear vertical modes show a quadratic dependence on the in-plane wave vector ($\omega \propto Q^2$). This appears to be related to the rigidity of two and more layers towards bending forces. This effect has been discussed previously in connection with layered compounds such as graphite.[61]

TABLE IV. The longitudinal acoustic impedance mismatches δ and interface reflection coefficients R of the four types of epitaxial overlayer systems.

	Ar/Ag(111)	Kr/Ag(111)	KBr/NaCl(001)	Na/Cu(001)	Pb/Cu(111)
δ	94.3%	88.0%	4.9%	90.2%	42.2%
R	0.89	0.79	0.02	0.82	0.27

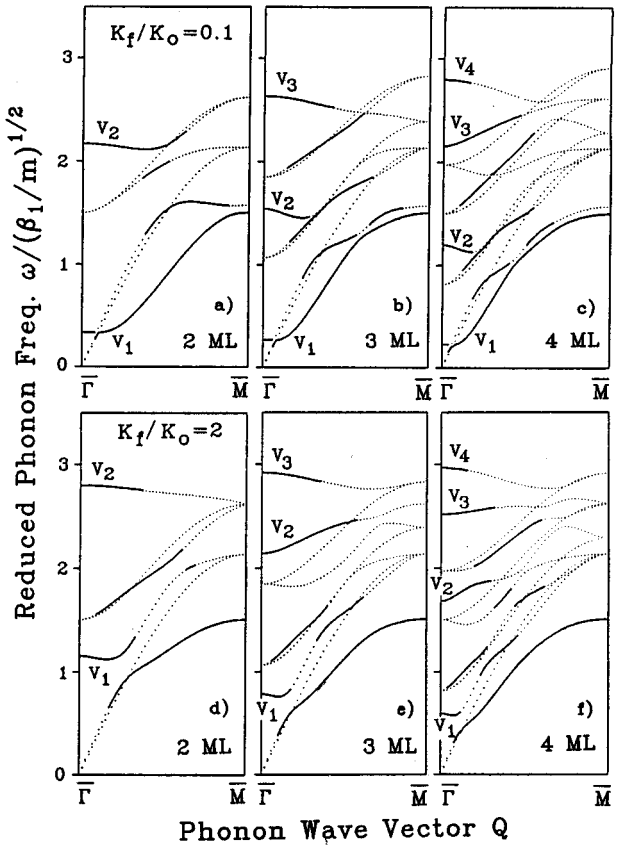

FIG. 8. Calculated phonon dispersion curves of fcc (100) overlayers on a rigid substrate along the $\overline{\Gamma M}$ direction. The solid lines indicate the modes that have predominantly vertical vibrational amplitudes at the surface. V_i $(i=1,\ldots,N)$ labels the ith mode polarized normal to the surface. For (a)–(c), $K_f/K_0=0.1$, (a) 2 ML, (b) 3 ML, (c) 4 ML. For (d)–(f), $K_f/K_0=2$ under the N open standing wave condition, (d) 2 ML, (e) 3 ML, (f) 4 ML. The frequencies are normalized by $\sqrt{\beta_1/m}$.

In Fig. 8 it is also apparent that the shear vertical model with the lowest frequency ω_1, which evolves to the Rayleigh wave for a thick overlayer, has the greatest positive slope, while the slopes of the shear vertical dispersion curves with $n>1$ decrease with increasing frequencies. This is attributed to the hybridization of the lower-frequency vertical modes with the longitudinal modes, which have a strong dispersion. The higher-frequency modes that can no longer hybridize are therefore flatter. This also explains why the dispersion curves of vertical modes are more flat for the open standing wave condition $(K_f/K_0=2)$ where the modes are pushed upwards in frequency than for the softer interface situation $(K_f/K_0=0.1)$. This suggests that the interface motions strongly affect the dispersion curves for these thin films.

Finally we note that for a given force constant ratio K_f/K_0, the slopes of vertical modes are also expected to depend on the interlayer structure as well as the direction of the wave vector. For example, in the case of a fcc thin film consisting of (001) layers shown in Fig. 9, the nearest-neighbor bonds located within one of the planes do not contribute to the vibrations normal to the surface, and only the four nearest-neighbor bonds between each pair of adjacent planes are involved in the vertical vibrations. Of these the

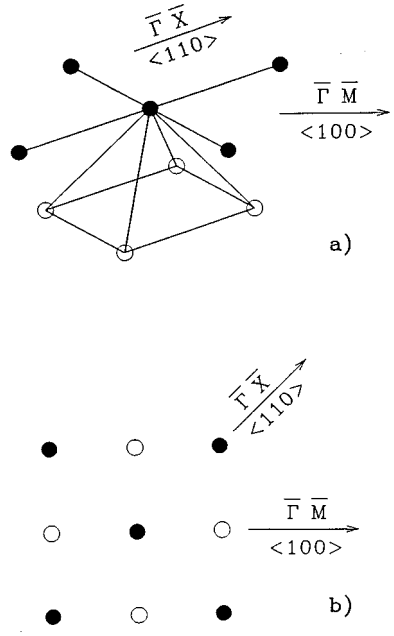

FIG. 9. Schematic diagrams of the first and second layers of a fcc (100) surface. Solid circles are the atoms at the surface, and the open circles are the atoms in the second layer. Solid lines connect the bonds between the nearest neighbors. (a) A three-dimensional picture. (b) A top view picture.

two bonds normal to the wave vector along the $\overline{\Gamma M}$ direction give no contribution to the corresponding dispersions. The dispersion is small since it results only from the coupling provided by the two other bonds, which have a projection in the direction of the wave vector. According to this model the dispersion should be larger along the $\overline{\Gamma X}$ direction.

III. REALISTIC CALCULATIONS FOR SODIUM FILMS ON COPPER (001)

A. Full dispersion curves for sodium films on a rigid substrate

To fully explain the HAS data for Na/Cu(001), the small dispersion of the open standing wave modes as reported in Ref. 37 has to be accounted for. This requires a more refined three-dimensional slab calculation with at least two radial force constants.[62] These were determined by a best fit of the bcc Na bulk phonon dispersion curves,[41] which yielded values of $\beta_1^{\mathrm{Na}}=3.70$ N/m between the first-neighbor atoms and $\beta_2^{\mathrm{Na}}=0.43$ N/m between the second-neighbor atoms. With these force constants the differences between measured and calculated phonon frequencies were less than 3.4%. As discussed above, because of the large acoustic mismatch (see Table I) the rigid substrate approximation is valid for this particular system.

HAS and LEED experiments suggest that the geometrical arrangement of the Na monolayers[34] evolves with increasing N from a quasihexagonal fcc (111) structure at the interface into a (110)-oriented bcc structure. The ideal bcc Na(110) structure is shown schematically in Fig. 10. The structure is very similar to a hexagonal fcc (111) lattice, since the difference between the first- and the second-neighbor distances in a bcc crystal is only about 15% with $r_1=0.886a_0$ and $r_2=a_0$, respectively, where a_0 is the lattice constant (see

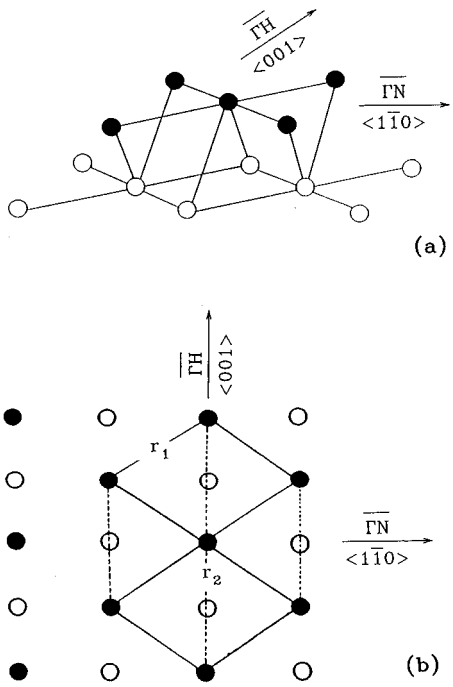

FIG. 10. Schematic diagrams of an ideal (110) surface of a bcc crystal. Solid circles are the atoms at the surface, and open circles the atoms in the second layer. Solid lines connect the bonds between the nearest neighbors, and dotted lines between the second neighbors. (a) A three-dimensional picture. (b) A top view picture.

Fig. 10). In the slab calculations we approximate the thin Na films by a uniform slab of bcc (110) planes. Then, according to Eq. (4), the interplanar force constant between adjacent bcc (110) atomic planes is calculated to be

$$K_0^{\mathrm{Na}}=\frac{4}{3}\beta_1^{\mathrm{Na}}+\beta_2^{\mathrm{Na}}=5.36\ \ \mathrm{N/m}. \tag{18}$$

Note that K_0^{Na} involves only the interactions between adjacent film planes. The interface interplanar force constant between the Na film and the extended rigid substrate $K_f^{\mathrm{Na(RS)}}$ is chosen according to the open standing wave interface condition ($K_f=2k_0$),

$$K_f^{\mathrm{Na(RS)}}=\beta^{\mathrm{Na(RS)}}=2K_0^{\mathrm{Na}}=10.72\ \ \mathrm{N/m}, \tag{19}$$

where $\beta^{\mathrm{Na(RS)}}$ is an effective radial force constant between an individual Na atom and the rigid Cu substrate.

The calculated dispersion curves along the $\overline{\Gamma N}$ direction of SBZ of Na(110) surface at different coverages, 2, 3, 4, 5, 10, 15, and 30 ML are shown in Figs. 11(a)–11(g), respectively. The frequencies of the vibrations normal to the surface (labeled with V_i, where $i=1,\ldots,N$) have the open standing wave sequences at the Γ point, in agreement with the previously obtained results with the linear chain model. In Fig. 11 the dispersion curves with predominantly shear vertical character are emphasized by the broad solid curves for $N\leqslant 5$ ML. The same general behavior holds for the thick films. In order to verify the open standing wave behavior at wave vectors approaching the zone boundary, the vertically polarized component of the phonon density of states [see Eq. (17)] at the surface is shown for the example of 5 ML for three different wave vectors in Fig. 12. As discussed in connection with Fig. 8 the lowest-frequency modes increase slightly with wave vector, whereas the high-frequency modes decrease. However, the dependence on wave vector is very small especially for the $n=2,3,\ldots$ modes. Thus, Figs. 11 and 12 show a trend towards a dispersionless behavior although not quite as flat as observed along the $\overline{\Gamma N}$ direction.

A possible simple explanation for this unique behavior can be found in the bcc structure. As discussed above in connection with the bulk phonons the dominant interaction in Na is between the nearest-neighbor atoms ($\beta_1^{\mathrm{Na}}=3.70$ N/m), whereas the interaction between the second-nearest-neighbor atoms ($\beta_2^{\mathrm{Na}}=0.43$ N/m) is only about 10% of the former. For each Na atom in the bcc (110) planes (see Fig. 10) the four nearest-neighbor bonds located in the plane do not contribute to the vibrations normal to the surface, and only the two nearest-neighbor bonds between atoms in adjacent planes are involved in the vertical vibrations. However, these two nearest-neighbor interplanar bonds give no contri-

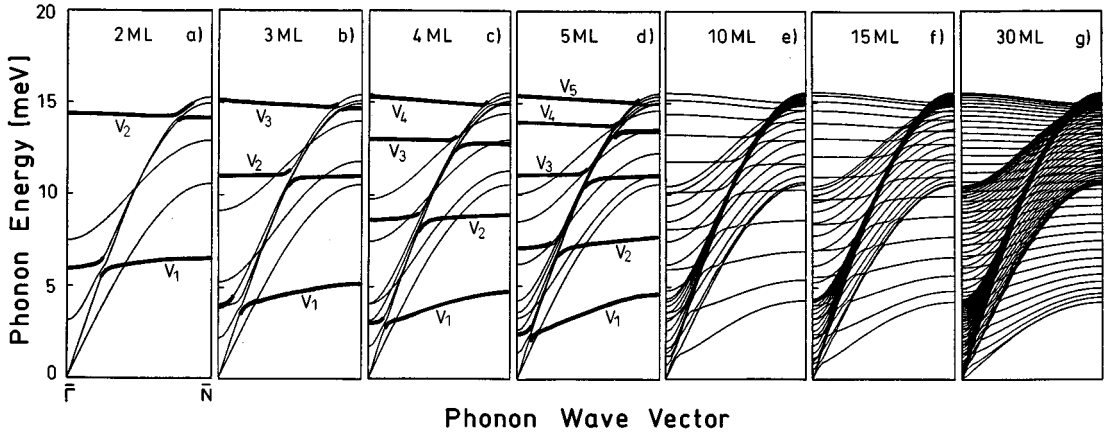

FIG. 11. Calculated phonon dispersion curves of bcc Na(110) overlayers on a rigid substrate along the $\overline{\Gamma N}$ direction with the force constants $\beta_1^{\mathrm{Na}}=3.70$ N/m, $\beta_2^{\mathrm{Na}}=0.43$ N/m, and $\beta^{\mathrm{Na(RS)}}=10.72$ N/m. (a) 2 ML, (b) 3 ML, (c) 4 ML, (d) 5 ML, (e) 10 ML, (f) 15 ML, and (g) 30 ML. The shear vertical vibrational modes for 2–5 ML coverages are emphasized by the boldface lines.

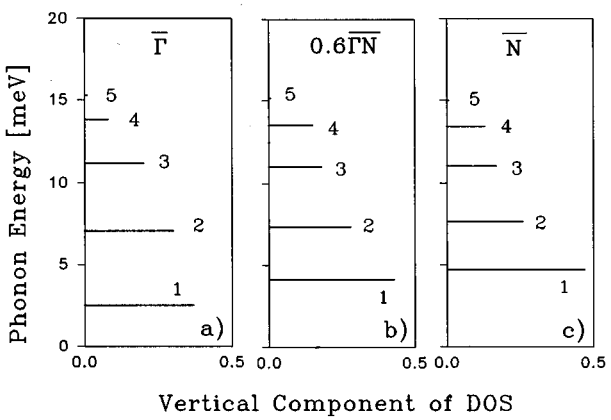

FIG. 12. Calculated phonon densities of states for the vertical component (horizontal bars) at the surface for a 5 ML Na(110) film on a rigid substrate. (a) At the $\bar{\Gamma}$ point. (b) At the $0.6\bar{\Gamma}\bar{N}$ point. (c) At the $\bar{N}$ point.

bution to the dispersions along the $\bar{\Gamma}\bar{N}$ direction because of being normal to this direction. Thus, only the very weak interaction between the second nearest neighbors contributes to the dispersion in this direction.

The theoretical results are qualitatively in good agreement with the measured data. However, a quantitative comparison with the experimental data shown in Table V indicates that the calculated frequencies of the open standing wave modes are generally 10%–20% smaller than the measured ones. This is likely to be due to the considerable strain in the layers resulting from the fact that the fcc (001) substrate has a different structure than the close-packed bcc Na(110) films.[63]

TABLE V. Comparison between the measured and calculated shear vertical vibrational frequencies at the $\bar{\Gamma}$ point for the Na/Cu (001) system. $\omega_n(N)$ denotes the nth shear vertical vibrational frequency at the $\bar{\Gamma}$ point in the system of N layers of sodium on Cu(001) surface ($n=1,2,\ldots,N$). The HAS measured data are from Ref. 34. Columns ''model A(I)'' and ''model A(II)'' are calculated by model A without and with adjustments of the bulk force constants, respectively. Model B [see Fig. 2(b)] calculations are made with the same intrafilm force constants for Na overlayers as in model A(II). All the values are in meV.

Modes	HAS data	Model A(I)	Model A(II)	Model B
$\omega_1(2)$	7.60	6.08	7.59	7.43
$\omega_1(3)$	5.10	4.05	5.06	5.05
$\omega_1(4)$	3.60	3.04	3.67	3.66
$\omega_2(4)$	10.40	8.61	10.60	10.71
$\omega_1(5)$	2.89	2.63	2.99	2.96
$\omega_2(5)$	8.42	7.09	8.62	8.71
$\omega_1(10)$	1.42	1.27	1.40	1.43
$\omega_2(10)$	4.21	3.67	4.43	4.42
$\omega_3(10)$	6.84	6.03	7.15	7.24
$\omega_4(10)$	9.46	8.23	10.0	9.96
$\omega_1(15)$	0.95	0.89	1.01	0.98
$\omega_2(15)$	2.97	2.28	2.91	2.96
$\omega_3(15)$	4.86	4.05	4.88	4.91
$\omega_4(15)$	6.49	5.57	6.75	6.86
$\omega_5(15)$	7.80	7.09	8.75	8.57

This is supported by the He atom diffraction measurements,[64] which reveal that whereas the first Na monolayer shows a $c(2\times2)$ structure, which has a lattice constant equal to that of the Cu substrate (3.61 Å), the second and third layers show a number of closely spaced satellites corresponding to a superstructure with a lattice constant of 3.65 Å. Low-energy electron diffraction experiments also indicate that the lattice constant evolves gradually from 3.61 Å to the value of 3.66 Å, which is still smaller than the lattice constant of a perfect Na lattice (3.71 Å).[63] Thus, the compression and structural distortion resulting from the Cu(001) substrate lead to a significant strain in the epitaxially grown Na films. This is favored by the anomalously small cohesive energy, the bulk modulus, and the shear modulus of sodium.[55] Strain induced by a lattice mismatch between substrate and film appears to be a universal phenomenon.[16–19]

To account for the existence of substrate-induced strain, we have adjusted the force constants between Na atoms in the epitaxial film in order to fit the measured dispersion curves. To simplify the problem, we assume that the intrafilm strain is uniformly distributed throughout the film, and the force constants between all the atoms of the slab are assumed to have the same average value. The best fit to measured dispersion curves is achieved by the force constant adjustments: $\Delta\beta_1^{\mathrm{Na}}=+1.63$ N/m ($\Delta\beta_1^{\mathrm{Na}}/\beta_1^{\mathrm{Na}}=+44\%$) and $\Delta\beta_2^{\mathrm{Na}}=+0.55$ N/m ($\Delta\beta_2^{\mathrm{Na}}/\beta_2^{\mathrm{Na}}=+128\%$). The adjusted Na film interplanar force constant is 8.08 N/m, which corresponds to a +51% increase when compared to the bulk value 5.36 N/m. In the fit the interface force constant is simultaneously adjusted so as to maintain the interface condition for open standing wave modes:

$$\Delta K_f^{\mathrm{Na(RS)}}=\Delta\beta^{\mathrm{Na(RS)}}=2\Delta K_2^{\mathrm{Na}}$$
$$=2[\tfrac{4}{3}\Delta\beta_1^{\mathrm{Na}}+\Delta\beta_2^{\mathrm{Na}}]=+5.44\ \text{N/m}. \qquad (20)$$

The adjusted interface force constant is determined to be 16.16 N/m, which is 51% larger than the value of 10.72 N/m for an ideal film. The adjusted interplanar force constant of 8.08 N/m and interface force constant of 16.16 N/m differ considerably from the values of 6.6 and 28.0 N/m, respectively, crudely estimated previously for the strained films using a much simpler model.[34]

With these force constant changes, the phonon dispersion curves of Na(110) overlayers on a rigid wall at different coverages, 2, 3, 4, 5, 10, 15, and 30 ML, are calculated along the $\bar{\Gamma}\bar{N}$ direction of SBZ of the Na(110) surface. The results for the dispersion curves are shown in Fig. 13. The numerical calculation of the frequencies at the $\bar{\Gamma}$ point for three different models are compared with all the experimental data for $N=2$, 3, 4, 5, 10, and 15 in Table V. The adjustment of the force constants within model A [see Fig. 2(a)] leads to a significant improvement in the agreement with the experimental $\bar{\Gamma}$-point data. For most of the frequencies in Table V the agreement is better than 2–3%. For the $\omega_2(10)$, $\omega_3(10)$, and $\omega_4(10)$ modes the calculated frequencies are too large by 5% and the largest error is found for the $\omega_5(15)$ mode, which is 12%.

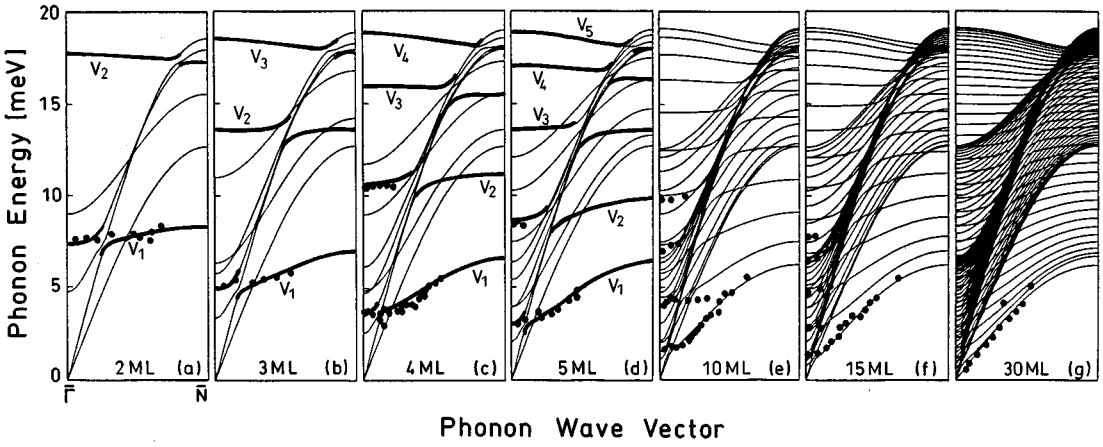

FIG. 13. Comparison of HAS data (solid circles) with calculated phonon dispersion curves of Na(110) overlayers on a rigid substrate along the $\overline{\Gamma N}$ direction with the force constant adjustments $\Delta\beta_1^{\mathrm{Na}}=+1.63$ N/m, $\Delta\beta_2^{\mathrm{Na}}=+0.55$ N/m, and $\Delta\beta^{\mathrm{Na(RS)}}=+5.44$ N/m. (a) 2 ML, (b) 3 ML, (c) 4 ML, (d) 5 ML, (e) 10 ML, (f) 15 ML and (g) 30 ML. The shear vertical vibrational modes for 2–5 ML coverages are emphasized by the boldface lines. The measurements are from Ref. 34 and only those points are shown that are relevant for the present theory.

B. The linear sodium chain on a vibrating copper substrate

To study the small coupling of overlayer and substrate vibrations for the Na/Cu(001) system, model B is applied in a realistic calculation for a linear chain of 200 Cu atoms with N Na atoms at each end ($N=1,2,3,...$). The nearest layer interplanar force constant in Na films is taken as 8.08 N/m, as determined in the above three-dimensional slab calculation with model A. For the fcc Cu substrate, the measured bulk phonon dispersion curves[42] can be reproduced very well with only one nearest-neighbor radial force constant $\beta_1^{\mathrm{Cu}}=28$ N/m.[49] Then, according to Eq. (4), the force constants between the Cu(001) planes are found to be $K_s^{\mathrm{Cu}}=2\beta_1^{\mathrm{Cu}}=56.0$ N/m for the nearest-neighbor planes, and no interaction for the other more distant planes. The only free parameter is the interplanar interface force constant K_f^{NaCu}, which can be determined by fitting the experimental data. In this linear chain system, the vibrations of the Na overlayers are all within the range of frequencies of the Cu substrate. We have calculated phonon densities of states at the surface versus the number of overlayers from 1 to 15. The best fit to the measured data is achieved with the interplanar interface force constant $K_f^{\mathrm{NaCu}}=15.0$ N/m and the corresponding phonon densities of states at the surface are shown in Fig. 14. As expected these densities of states are similar to the open standing wave state densities calculated with the rigid substrate approximation shown in Fig. 7(a). By comparing the results of model B with that of model A, the error in fitting the interface force constant introduced by the rigid substrate approximation in model A for the Na/Cu(001) system is identified as 7.7%. Hence, this realistic calculation has confirmed that the rigid substrate approximation is a useful description of the Na/Cu(001) system. The calculated frequencies from model B are also listed in Table V. They differ by 2% and agree better with the measured data than the model A(II) calculations as expected from the result presented in Sec. II. In addition, in Fig. 14 one can see that the half width of the peaks is larger in the lower-frequency modes, especially for the thin films (N small). This feature reveals that the lower-frequency modes are relatively more strongly coupled with the substrate vibrations.

IV. CONCLUSIONS

In this work, we have carried out a systematic theoretical analysis of the vibrational modes at the Γ point of epitaxial thin-film systems. A simple linear chain model has been shown to be capable of explaining the measured phonon frequencies at the Γ point as a function of film thickness for the four different epitaxial systems Na/Cu(001),[34] Pb/Cu(111),[35] Ar(Kr)/Ag(111),[21,22] and KBr/NaCl(001).[33] All four films are softer than the corresponding substrate (see Table I). The model shows that the decrease of the frequencies with increasing film thickness depends sensitively on the ratio of the

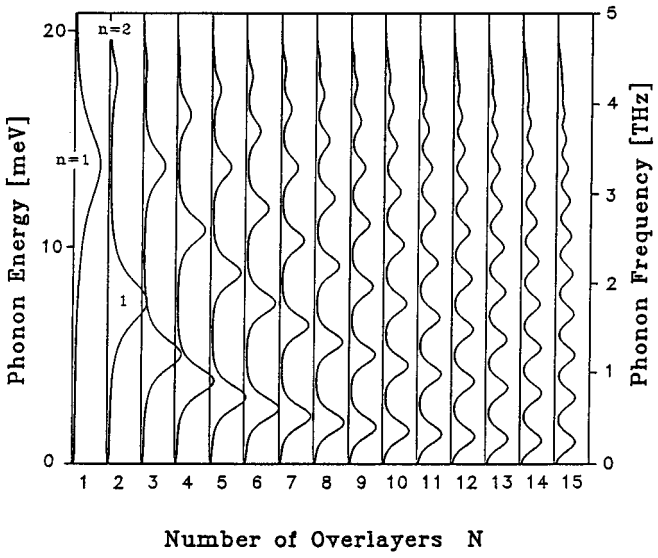

FIG. 14. Calculated phonon densities of states for the vertical component at the surface of a linear chain Na/Cu/Na. The Cu(001) substrate has 200 layers, while the number of Na(110) overlayers varies from 1 to 15.

film interlayer force constant to the force constant at the interface to the rigid substrate (see Table II). The theory furnishes a simple explanation of the HAS measured open standing wave frequency sequence in Na epitaxial thin films on Cu(001) in terms of a special relationship between the interface and intrafilm interactions within the framework of the force constant models. The effect of the acoustic impedance mismatch of the film to the substrate is also discussed. In cases of a large mismatch such as in Ar(Kr)/Ag(111) and Na/Cu(001) the coupling to the substrate modes can be neglected. In addition, the full dispersion curves for 2–30 ML Na on Cu(001) have been calculated for bcc Na(110) films. Good agreement with experimental results can only be obtained by increasing both the interlayer film force constant and the corresponding interface constant by 50.7%. This increase is consistent with the observation of structural mismatch at the interface, which is responsible for the strong increase in the film force constants. The full dispersion curves in the $\overline{\Gamma N}$ direction show that the nearly dispersionless behavior is caused by the special interlayer structure of Na bcc films. The present work shows that the frequencies at the $\overline{\Gamma}$ point contain considerable information on both strain within the intralayers and the relative strength of the interface force constant.

More work is needed to understand the behavior in the case of films that are stiffer than the substrate. For both cases of softer and stiffer substrates the influence of the substrate vibrations in situations where the acoustic impedance mismatch is not large still needs to be examined in detail.

ACKNOWLEDGMENTS

N.S.L. and P.R. gratefully acknowledge the support of the Max-Planck Society. We thank D. Paulmann for help with some of the calculations. The authors thank G. Benedek (Milano), J. G. Skofronick (Florida), J. R. Manson (Clemson), and F. W. de Wette (Austin) for many valuable critical discussions. We would like to thank V. Celli (Virginia) for suggesting the derivation of some of the equations in Sec. II A. N.S.L. is also grateful to the support of the National Science Foundation through Grant No. EHR-9108764.

*Present address: Department of Physics, University of Louisville, Louisville, Kentucky 40292.

†Present address: Fritz-Haber-Institut der Max-Planck-Gesellschaft, Faradayweg 4-6, 14195 Berlin-Dahlem, Germany.

[1] S. Yoshida, CRC Crit. Rev. Solid State Mater. Sci. **11**, 287 (1985).

[2] M. H. Herman and H. Sitter, *Molecular Beam Epitaxy* (Springer-Verlag, Berlin, 1989).

[3] A. L. Wachs, A. P. Shapiro, T. C. Hsieh, and T. C. Chiang, Phys. Rev. B **33**, 1460 (1986).

[4] S. A. Lindgren and L. Wallden, Phys. Rev. Lett. **59**, 3003 (1987).

[5] S. A. Lindgren and L. Wallden, Phys. Rev. Lett. **61**, 2894 (1988).

[6] S. A. Lindgren and L. Wallden, Phys. Rev. B **38**, 3060 (1988).

[7] S. A. Lindgren and L. Wallden, J. Phys. Condens. Matter **1**, 2151 (1989).

[8] A. Hamawi, S. A. Lindgren, and L. Wallden, Phys. Scr. **T39**, 339 (1991).

[9] A. Hamawi, S. A. Lindgren, C. Svensson, and L. Wallden, Acta Phys. Pol. **A81**, 7 (1992).

[10] T. Miller, A. Samsavar, G. E. Franklin, and T. C. Chiang, Phys. Rev. Lett. **61**, 1404 (1988).

[11] V. De Renzi, M. G. Betti, and C. Mariani, Phys. Rev. B **48**, 4767 (1993).

[12] R. C. Jaklevic and J. Lambe, Phys. Rev. B **12**, 4146 (1975).

[13] H. Iwasaki, B. T. Jonker, and R. L. Park, Phys. Rev. B **32**, 643 (1985).

[14] M. Jalochowski, E. Bauer, H. Knoppe, and G. Lilienkamp, Phys. Rev. B **45**, 13 607 (1992).

[15] B. J. Hinch, C. Koziol, J. P. Toennies, and G. Zhang, Europhys. Lett. **10**, 341 (1989).

[16] J. E. Black, A. Janzen, and P. Bopp, Surf. Sci. **259**, 371 (1991).

[17] L. Yang, T. S. Rahman, and J. E. Black, Surf. Sci. **278**, 407 (1992).

[18] D. D. Koleske and S. J. Sibener, Surf. Sci. **290**, 179 (1993).

[19] A. J. Schell-Sorokin and R. M. Tromp, Phys. Rev. Lett. **64**, 1039 (1990).

[20] H. L. Störmer, Surf. Sci. **132**, 519 (1983).

[21] K. D. Gibson and S. J. Sibener, Phys. Rev. Lett. **55**, 1514 (1985).

[22] K. D. Gibson, S. J. Sibener, Burl M. Hall, D. L. Mills, and J. E. Black, J. Chem. Phys. **83**, 4256 (1985).

[23] H. Jonsson and J. H. Weare, Surf. Sci. **181**, 495 (1987).

[24] K. Kern, P. Zeppenfeld, R. David, and G. Comsa, Phys. Rev. B **35**, 886 (1987).

[25] B. Hall, D. L. Mills, P. Zeppenfeld, K. Kern, U. Becher, and G. Comsa, Phys. Rev. B **40**, 6326 (1989).

[26] W. Daum, J. Electron. Spectrosc. Relat. Phenom. **44**, 271 (1987).

[27] W. Daum, C. Stuhlmann, and H. Ibach, Phys. Rev. Lett. **60**, 2741 (1988).

[28] M. H. Mohamed, J. S. Kim, and L. L. Kesmodel, Surf. Sci. **220**, L687 (1989).

[29] C. Stuhlmann and H. Ibach, Surf. Sci. **219**, 117 (1989).

[30] M. H. Mohamed, J. S. Kim, and L. L. Kesmodel, Phys. Rev. B **40**, 1305 (1989).

[31] Y. Chen, S. Y. Tang, J. S. Kim, M. H. Mohamed, and L. L. Kesmodel, Phys. Rev. B **43**, 6788 (1991).

[32] G. W. Farnell and E. L. Adler, in *Physical Acoustics*, edited by W. P. Mason and R. N. Tharston (Academic, New York, 1972), Vol. IX.

[33] S. A. Safron, G. G. Bishop, J. Duan, E. S. Gillman, J. G. Skofronik, N. S. Luo, and P. Ruggerone, J. Phys. Chem. **97**, 2270 (1993).

[34] G. Benedek, J. Ellis, A. Reichmuth, P. Ruggerone, H. Schief, and J. P. Toennies, Phys. Rev. Lett. **69**, 2951 (1992).

[35] N. S. Luo, P. Ruggerone, J. P. Toennies, and Ge Zhang (unpublished); Ge Zhang, Ph.D. thesis, Max-Planck-Institut für Strömungsforschung, Göttingen, 1990.

[36] *American Institute of Physics Handbook*, 3rd ed., edited by D. E. Gray (McGraw-Hill, New York, 1972).

[37] Y. Fujii, N. A. Lurie, R. Pynn, and G. Shirane, Phys. Rev. B **10**, 3647 (1974).

[38] J. Skalyo, Jr., Y. Endoh, and G. Shirane, Phys. Rev. B **9**, 1797 (1974).

[39] H. Bilz and W. Kress, *Phonon Dispersion Relations in Insulators*, Springer Series in Solid State Sciences Vol. 10 (Springer-Verlag, Berlin, 1979).

[40] W. Drexel, Z. Phys. **255**, 281 (1972).

[41] A. D. B. Woods, B. N. Brockhouse, R. H. March, and A. T. Stewers, Phys. Rev. **128**, 1112 (1962).
[42] R. M. Nicklow, G. Gilat, H. G. Smith, L. J. Raubenheimer, and M. K. Wilkinson, Phys. Rev. **164**, 922 (1967).
[43] B. N. Brockhouse, T. Arose, G. Cagliotti, K. R. Rao, and A. D. B. Woods, Phys. Rev. **128**, 1099 (1962).
[44] J. D. White, J. Cui, M. Strauss, R. D. Diehl, F. Ancilotto, and F. Toigo, Surf. Sci. **307**, 1134 (1994).
[45] G. Brusdeylins, N. S. Luo, P. Ruggerone, D. Schmicker, J. P. Toennies, R. Vollmer, and Th. Wach, Surf. Sci. **272**, 358 (1992).
[46] S. Schmidt, Diplom thesis, University of Göttingen, 1992.
[47] N. Bunjes, Diplom thesis, University of Göttingen, 1994.
[48] The same behavior has also been found for Cs/Cu(111), E. Hulpke and A. Reichmuth, Phys. Rev. B **53**, 13 901 (1996).
[49] C. Kaden, P. Ruggerone, J. P. Toennies, G. Zhang, and G. Benedek, Phys. Rev. B **46**, 13 509 (1992).
[50] G. Benedek, J. Ellis, N. S. Luo, A. Reichmuth, P. Ruggerone, and J. P. Toennies, Phys. Rev. B **48**, 4917 (1993).
[51] N. Bunjes, N. S. Luo, P. Ruggerone, J. P. Toennies, and G. Witte, Phys. Rev. B **50**, 8897 (1994).
[52] A. Franchini, V. Bortolani, G. Santoro, V. Celli, A. G. Eguiluz, J. A. Gaspar, M. Gester, A. Lock, and J. P. Toennies, Phys. Rev. B **47**, 4691 (1993).
[53] P. Senet (private communication).
[54] N. S. Luo, P. Ruggerone, J. P. Toennies, G. Benedek, and V. Celli, J. Electron. Spectrosc. Relat. Phenom. **64/65**, 755 (1993).
[55] C. Kittel, *Introduction to Solid State Physics*, 5th ed. (Wiley, New York, 1976).
[56] J. P. Toennies, in *Solvay Conference on Surface Science*, edited by F. W. de Wette, Springer Series in Surface Sciences Vol. 14 (Springer-Verlag, Berlin, 1988).
[57] J. de Launay, in *Solid State Physics*, edited by F. Seitz and D. Turnball (Academic, New York, 1956).
[58] A. Reichmuth, Ph.D. thesis, Department of Physics, Cambridge University, UK, 1994.
[59] The acoustic impedance Z is equal to the mass density ρ times the longitudinal sound velocity v. We have $Z=\rho v$ and $\rho=m/V^*$, where m is the mass of an atom and V^* the volume per atom. Moreover, the longitudinal sound velocity v of a linear chain with the interplanar force constant K can be written as $v=\sqrt{4K/m}(a^*/2)\cos(q_z/2)$ according to Eq. (16). Therefore, the acoustic impedance Z is proportional to $\sqrt{Km}$.
[60] B. A. Auld, *Acoustic Fields and Waves in Solids* (Wiley, New York, 1973).
[61] P. Brüesch, *Phonons, Theory and Experiments I* (Springer-Verlag, Berlin, 1982), p. 150.
[62] J. E. Black, D. A. Campbell, and R. F. Wallis, Surf. Sci. **115**, 161 (1982).
[63] H. Schief, Diplom thesis, University of Göttingen, 1990.
[64] A. Reichmuth, Diplom thesis, University of Göttingen, 1991.